nature chemistry

ARTICLES

https://doi.org/10.1038/s41557-021-00748-5

Check for updates

Olefin metathesis-based chemically recyclable polymers enabled by fused-ring monomers

Devavrat Sathe[1], Junfeng Zhou[1], Hanlin Chen[1], Hsin-Wei Su[1], Wei Xie[1], Tze-Gang Hsu[1], Briana R. Schrage[2], Travis Smith[1], Christopher J. Ziegler[2] and Junpeng Wang[1]✉

A promising solution to address the challenges in plastics sustainability is to replace current polymers with chemically recyclable ones that can depolymerize into their constituent monomers to enable the circular use of materials. Despite some progress, few depolymerizable polymers exhibit the desirable thermal stability and strong mechanical properties of traditional polymers. Here we report a series of chemically recyclable polymers that show excellent thermal stability (decomposition temperature >370 °C) and tunable mechanical properties. The polymers are formed through ring-opening metathesis polymerization of cyclooctene with a *trans*-cyclobutane installed at the 5 and 6 positions. The additional ring converts the non-depolymerizable polycyclooctene into a depolymerizable polymer by reducing the ring strain energy in the monomer (from 8.2 kcal mol^{-1} in unsubstituted cyclooctene to 4.9 kcal mol^{-1} in the fused ring). The fused-ring monomer enables a broad scope of functionalities to be incorporated, providing access to chemically recyclable elastomers and plastics that show promise as next-generation sustainable materials.

Synthetic polymers, including synthetic rubber and synthetic plastics, have been used in nearly every aspect of our daily lives. The dominance of synthetic polymers is largely driven by their excellent stability and processability as well as their versatile mechanical properties. However, due to their high durability, waste materials composed of these polymers have accumulated in the ocean and have caused serious concerns for marine ecosystems[1]. In addition, because 90% of these polymers are derived from finite fossil feedstocks, the production of these materials is unsustainable if they cannot be recycled and reused[2]. Efforts to address these issues include the development of biodegradable polymers and mechanical recycling. However, most biodegradable polymers that can be degraded in artificial environments do not undergo efficient degradation in seawater, giving rise to new environmental consequences[3]. Mechanical recycling of polymers typically results in substantial loss of quality, and the recycled material is not suitable for high-performance applications[4]. A particularly attractive strategy is to develop chemically recyclable polymers that can depolymerize into their constituent monomers for recycling and repolymerization[5,6]. Circular use of the materials not only will help to preserve finite natural resources but also can address end-of-life issues for such materials.

To replace currently available commercial polymers, depolymerizable polymers need to match or exceed the properties of the current ones. With exceptions, polymerization is typically favoured in enthalpy ($\Delta H < 0$) and disfavoured in entropy ($\Delta S < 0$). The temperature at which the entropic loss will offset the enthalpic gain is defined as the ceiling temperature T_c, and depolymerization is favoured when the temperature is above T_c. Common polymers such as polyolefins have high T_c values, and their depolymerization is either costly in terms of energy or is susceptible to decomposition. Classical low-T_c polymers such as poly(olefin sulfones)[7,8], poly(α-methyl styrene)[9] and polyaldehydes[10] lack high thermal and chemical stability, and their use has been limited to certain specific applications such as transient electronics[11–13]. A promising strategy to address the stability issues is to develop polymers that only undergo efficient depolymerization in the presence of a catalyst. In other words, without the catalyst, the polymer is in a kinetic trap so that it will stay intact even when the temperature is above T_c. Recently, it has been shown that ring-opening polymerization of certain cyclic monomers—such as cyclic esters, cyclic carbonates and cyclic olefins—can lead to polymers that can depolymerize into the corresponding monomers in the presence of catalysts but show high thermal stability when the catalysts are removed[6]. For example, Chen and coworkers have shown that a poly(γ-butyrolactone) required heating overnight at 300 °C to be depolymerized, but the depolymerization temperature was reduced to 120 °C when a $ZnCl_2$ catalyst was added[14].

Among the catalytically depolymerizable polymers, a particularly attractive system is the one that is based on olefin metathesis[15]. Since olefin metathesis does not occur without a catalyst, unintended depolymerization can be prevented by removing the catalyst. In addition, metathesis is compatible with a wide variety of functional groups and can be conducted in mild or ambient reaction conditions[15]. Metathesis-based depolymerizable polymers are typically made via ring-opening metathesis polymerization (ROMP)[16] of cycloalkenes and can depolymerize through ring-closing metathesis (RCM)[17] to form the corresponding monomers. Compared to the ring-opening polymerization that is based on cyclic esters and cyclic carbonates, ROMP enables the production of polymers with hydrocarbon backbones, which have greater hydrolytic and thermal stability. However, up to now, demonstrations of depolymerizable ROMP polymers have been limited to polymers of five-membered cycloalkenes, namely the polypentenamers[18]. As polypentenamers are typically amorphous polymers with glass transition temperatures (T_g) below or near room temperature[18], they are not suitable for plastics applications where glassy or semicrystalline polymers are needed. Furthermore, the controlled polymerization of cyclopentene is challenging: the reported cases of controlled polymerization of cyclopentene require that the conversion be limited to a low

[1]School of Polymer Science and Polymer Engineering, University of Akron, Akron, OH, USA. [2]Department of Chemistry, University of Akron, Akron, OH, USA. ✉e-mail: jwang6@uakron.edu

threshold (<20%)[19] or that it be conducted in a variable-temperature fashion[20].

To address the needs for more robust depolymerizable ROMP polymers, we looked into other cyclic olefins. Because cyclopropene and cyclobutene are highly strained, with reported ring strain energies (RSEs) of 54.5 and 30.6 kcal mol^{-1}, respectively[21], the depolymerization of their ROMP polymers is not feasible. The ring strain of cyclohexene is too low to achieve a successful ROMP[22]. Of the seven-membered to twelve-membered cyclic olefins, the eight-membered one is particularly attractive because functionalized cyclooctenes can be made from 1,5-cyclooctadiene, an inexpensive, commercially available material. As a result, poly(cyclooctenes) have been one of the most extensively employed poly(cycloalkenes)[23]. In addition, the *Z*-alkene in cyclooctene can be inverted into an *E*-alkene to increase the RSE (the RSE of *trans*-alkene cyclooctene is 16.7 kcal mol^{-1} (ref. [21])) and enable living polymerization[24,25]. However, compared to cyclopentene (RSE = 5.2 kcal mol^{-1}), the higher ring strain of cyclooctene (RSE = 8.2 kcal mol^{-1}) precludes the depolymerization of polycyclooctene; note that because different RSEs have been reported for cyclooctene, we use our calculated values throughout the text for consistency. We hypothesized that if the RSE of cyclooctene could be reduced to a level comparable to that of cyclopentene, the corresponding polymer would undergo similar depolymerization.

It has been shown that the ring strain of cyclooctene can be lowered by a fused ring at the 5 and 6 positions and that the stereochemistry of the fused ring plays a critical role. For example, Coates and coworkers showed that an imidazolium-fused cyclooctene monomer only afforded macrocyclic oligomers under typical ROMP conditions, suggesting that the imidazolium-fused ring lowers the ring strain of cyclooctene[26]. Scherman et al. showed that a cyclooctene monomer with a *trans*-fused acetonide afforded much lower yield in polymerization than a *cis*-acetonide cyclooctene monomer (15% versus 80% when the polymerization was conducted at 1.0 M monomer concentration), indicating that the *trans*-fused acetonide cyclooctene has a lower RSE than that of its *cis* analogue[27]. These studies suggest that an appropriate fused ring may lower the ring strain of cyclooctene to enable the depolymerization of the corresponding ROMP polymer (Fig. 1a).

Results and discussion

Calculations of RSEs. To identify a fused ring that can lower the ring strain of cyclooctene to the above-mentioned target, we calculated the RSEs of cyclooctenes with three-, four-, five- and six-membered rings fused at the 5 and 6 positions, including both *cis* and *trans* isomers (Fig. 1b). The computation of RSE was conducted by calculating the enthalpy change of the RCM reaction shown in Fig. 1c using density functional theory at the B3LYP/6-31G(d,p) level, which provided reasonable predictions for the RSEs of cyclic olefins[22].

Based on the difference in RSE between the fused rings and the unsubstituted cyclooctene (RSE = 8.2 kcal mol^{-1}), the calculated results can be sorted into three groups:

1. RSEs that are higher than that of the virgin cyclooctene, including *cis*-cyclopropane-, *trans*-cyclopropane- and *cis*-cyclobutane-fused cyclooctenes
2. Fused rings with slightly decreased ring strain, including *cis*-cyclopentane-, *cis*-cyclohexane- and *trans*-cyclohexane-fused cyclooctenes
3. Cycloalkane-fused cyclooctenes having the lowest RSEs and having RSEs that are lower than or comparable to that of cyclopentene (RSE = 5.2 kcal mol^{-1}), including *trans*-cyclobutane- and *trans*-cyclopentane-fused cyclooctenes

The calculated RSEs suggest that the ROMP polymers of the *trans*-cyclobutane- and *trans*-cyclopentane-fused cyclooctenes would undergo catalytic depolymerization in a way similar to polypentenamers. Because of the synthetic convenience of accessing cyclobutane- and cyclopropane-fused cyclooctenes from 1,5-cyclooctadiene, we employed these cycloalkane-fused cyclooctenes for our experimental and control studies.

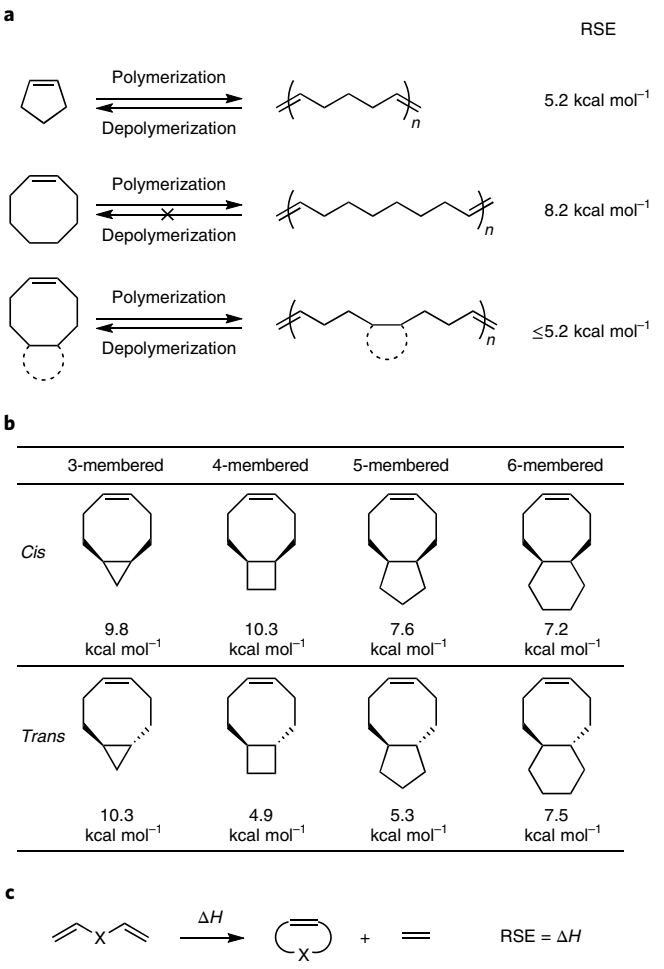

Fig. 1 | Identifying the appropriate ring that lowers the RSE for cyclooctene to enable depolymerization of the corresponding polymer. **a**, Polycyclopentene is depolymerizable, whereas polycyclooctene is not. The difference is caused by a higher RSE in cyclooctene. An appropriate ring (shown as a dashed line) lowers the RSE of cyclooctene to a level that is lower than or comparable to that of cyclopentene, enabling depolymerization of the polymer. **b**, The calculated RSEs for cyclooctene with 3-, 4-, 5- and 6-membered rings both *cis*- and *trans*-fused at the 5 and 6 positions. **c**, The generalized ring-closing metathesis reaction used to calculate the RSE of a cyclic olefin: the RSE for the cyclic olefin is essentially the enthalpy change for the ring-closing metathesis that affords the cyclic olefin.

Monomer synthesis. Recently, in an effort to control polymer degradation through mechanochemical activation, we synthesized **M1** through a photochemical [2 + 2] cycloaddition of 1,5-cyclooctadiene and maleic anhydride followed by $LiAlH_4$ reduction (Fig. 2a)[28]. Note that the cyclobutane in **M1** is *trans*-fused to the cyclooctene, indicating a *cis*-to-*trans* isomerization of the alkene prior to cycloaddition. Similar inversion of stereochemistry has been observed in other systems[29–32]. Importantly, the moiety of *trans*-cyclobutane-fused cyclooctene (*t*CBCO) is exactly the target moiety we are aiming for. Aside from lactone, *t*CBCOs with other functional groups—including the diesters **M2a** and **M2b**, the diether **M3** and the imide **M4**—were conveniently derived from the intermediate anhydride **1**.

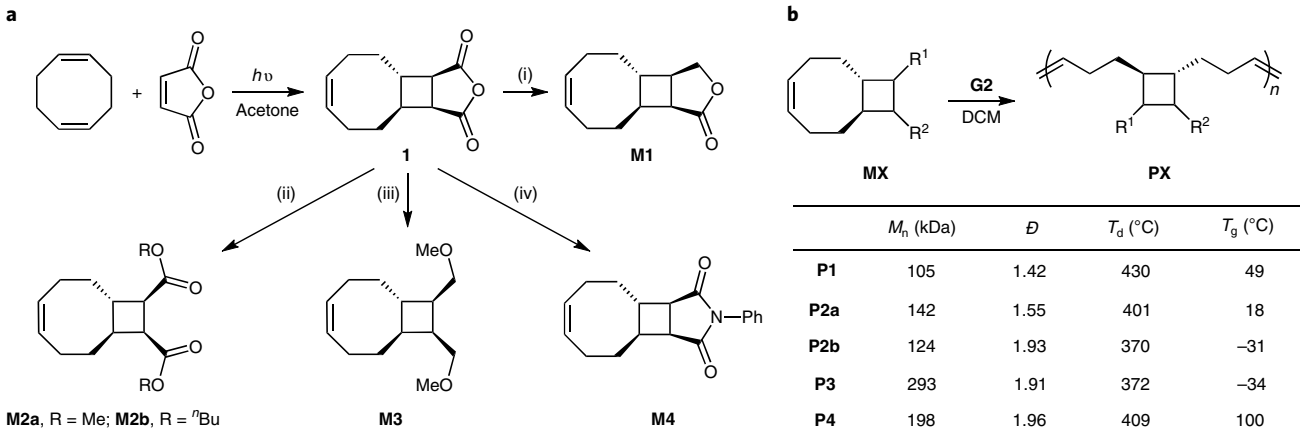

	M_n (kDa)	$Đ$	T_d (°C)	T_g (°C)
P1	105	1.42	430	49
P2a	142	1.55	401	18
P2b	124	1.93	370	–31
P3	293	1.91	372	–34
P4	198	1.96	409	100

Fig. 2 | Synthesis and characterization of the *t*CBCO monomers and polymers. a, Synthetic scheme of the *t*CBCO monomers. Photochemical [2 + 2] cycloaddition of 1,5-cyclooctadiene and maleic anhydride affords the anhydride **1**, which can be readily converted to **M1**, **M2**, **M3** and **M4** through conditions (i), (ii), (iii) and (iv), respectively. (i) 0.5 equiv. $LiAlH_4$, THF. (ii) **M2a**: MeOH, reflux; MeOH, EDC, DMAP, DCM. **M2b**: NaOH, H_2O, 60 °C; 1-butanol, EDC, DMAP, DCM. (iii) 1.0 equiv. $LiAlH_4$, THF; NaH, MeI, THF. (iv) Aniline, acetone; sodium acetate, acetic anhydride, 100 °C. **b**, Synthetic scheme, molecular weight information and thermal characterization data of the *t*CBCO polymers. THF, tetrahydrofuran; EDC, 1-ethyl-3-(3-dimethylaminopropyl)carbodiimide hydrochloride; DMAP, 4-dimethylaminopyridine; DCM, dichloromethane.

Polymerization thermodynamics. A high monomer concentration was found to be essential for the ROMP of these monomers, as low monomer concentrations resulted in low conversions. In addition, the conversion was also influenced by the temperature. For example, a xylene solution of 1.0 M **M2a** with 1.0 mol% Grubbs' second-generation catalyst (**G2**) resulted in 67% conversion when the reaction reached equilibrium at 19 °C. The equilibrium conversion was lowered to 53% when the reaction temperature was raised to 65 °C. From the conversions of the polymerization conducted at various temperatures (Supplementary Figs. 1 and 2), we obtained the thermodynamic data for **M2a** at 1.0 M: $\Delta H = -1.7$ kcal mol^{-1} and $\Delta S = -3.6$ cal mol^{-1} K^{-1}. Similarly, the ΔH (1.0 M) and ΔS (1.0 M) for **M4** we obtained were −2.8 kcal mol^{-1} and −4.9 cal mol^{-1} K^{-1}, respectively. While the experimental enthalpy changes confirmed the predicted low RSEs for these monomers, the experimental values are ~2–3 kcal mol^{-1} lower than the calculated ones (which are 5.0 kcal mol^{-1} and 5.1 kcal mol^{-1} for **M2a** and **M4**, respectively). The discrepancy could be due to the presence of a small fraction of cyclic oligomers in the polymerization mixture, as evidenced by gel permeation chromatography (GPC; Supplementary Figs. 3 and 4) and mass spectrometry (MS; Supplementary Fig. 5), while the RSEs were calculated solely using the energies of the acyclic diene. In addition, the entropy changes for these monomers are substantially lower than that for cyclopentene ($\Delta S = -18.5$ cal mol^{-1} K^{-1}). The reduced entropy change can be attributed to the lower loss in translational entropy for the larger-sized monomers and the higher gain in rotational entropy due to the higher number of freed bonds in the eight-membered ring that were attained through the ring-opening reaction. Compared to cyclopentene, the lower entropy loss for the polymerization of *t*CBCO monomers compensates the lower enthalpy gain and makes the polymerization favourable at high monomer concentrations. For example, at 25 °C and 1.0 M concentration, the Gibbs free energy values (ΔG) for polymerization of **M2a** and **M4** are −0.63 kcal mol^{-1} and −1.33 kcal mol^{-1}, respectively, which are more favourable than that for cyclopentene ($\Delta G = -0.087$ kcal mol^{-1}). The ceiling temperatures for **P2a**, **P4** and polypentenamer at 1.0 M are 199 °C, 295 °C and 30 °C, respectively. In addition, many functional groups on the 3 position of cyclopentene could reduce the ceiling temperature to values below room temperature, making the monomers challenging to polymerize[18]. Compared to polypentenamer, the favourable ceiling temperatures of the *t*CBCO system can enable the preparation of *t*CBCO polymers of a variety of functionalities through ROMP.

Polymer synthesis. The monomers were subjected to ROMP conditions with ~2 M monomer concentration in dichloromethane and **G2** as the initiator, yielding the polymers **P1**, **P2a**, **P2b**, **P3** and **P4** at high conversions (>80%; Fig. 2b). The number average molecular weight M_n, dispersity $Đ$, glass transition temperature T_g and decomposition temperature T_d (defined as the temperature at which 5% weight loss occurs) for each polymer are shown in Fig. 2b. Polymers with high molecular weights ($M_n > 100$ kDa) were obtained for all polymers. The high dispersities ($Đ > 1.5$) are comparable to those for other ROMP polymers of low-strain monomers[22,33]. As stated above, an advantage of the eight-membered cycloalkene is that the *cis*-alkene can be inverted to a *trans*-alkene, which is highly strained and is suitable for living ROMP. We converted **M2a** into ***E*-M2a** through photoisomerization by following the protocol demonstrated by Fox and coworkers[34]. A controlled ROMP was conducted by employing the conditions developed by Grubbs and coworkers, where Grubbs' first-generation catalyst (**G1**) and excess triphenylphosphine were used[24]. **P2a**′ with high molecular weight and low dispersity ($M_n = 94.7$ kDa, $Đ = 1.23$) was obtained at high conversion (>95%) even when the ROMP was conducted at a monomer concentration of 0.25 M.

Depolymerization studies. To test the capability of depolymerization, the polymers were dissolved in chloroform ($CHCl_3$) or deuterated chloroform ($CDCl_3$) at a concentration of 25 mM ([olefin] = 25 mM) and heated at 50 °C in the presence of 1 mol% **G2** for 2 h. The *t*CBCO polymers all underwent >90% depolymerization to form the corresponding monomers (Supplementary Table 1), as supported by observations obtained via proton nuclear magnetic resonance (^{1}H NMR; Fig. 3a–c and Supplementary Figs. 6–8), GPC (Supplementary Fig. 9) and MS (Supplementary Fig. 10). In addition, monomer **M2a**, which was isolated from the depolymerization mixture of **P2a** (characterization data of the isolated products shown in Supplementary Figs. 11–14), was subjected to the ROMP conditions described above and yielded polymers of high molecular weight ($M_n = 71$ kDa, $Đ = 1.53$; Supplementary Figs. 15 and 16).

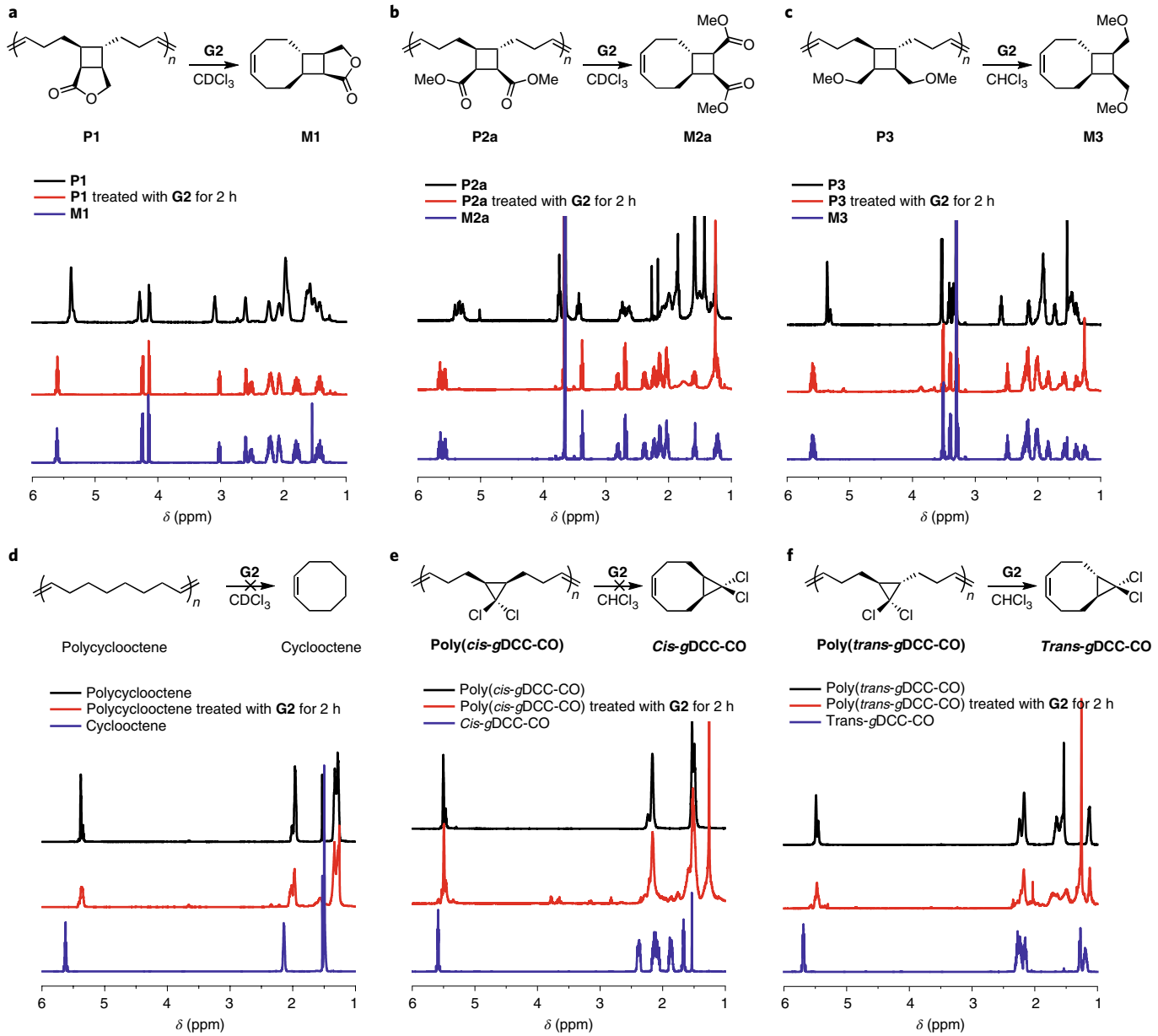

Fig. 3 | Depolymerization studies of *t*CBCO polymers. a–f, The ^{1}H NMR spectra for **P1** (**a**), **P2a** (**b**), **P3** (**c**), polycyclooctene (**d**), poly(*cis*-*g*DCC-CO) (**e**) and poly(*trans*-*g*DCC-CO) (**f**) before (in black) and after (in red) 2 h of heating the polymer solution (solvent, chloroform or deuterated chloroform; [olefin] = 25 mM) at 50 °C in the presence of Grubbs's second-generation catalyst (**G2**). The ^{1}H NMR spectra of the corresponding monomers are shown (in blue) as references. The red spectra (polymer treated with **G2**) and blue spectra (monomer) are nearly identical for *t*CBCO polymers, indicating complete depolymerization (**a**–**c**); however, the spectra are distinct for polycyclooctene, poly(*cis*-*g*DCC-CO) and poly(*trans*-*g*DCC-CO), suggesting no depolymerization occurred (**d**–**f**).

By contrast, when exposed to the same conditions, polycyclooctene did not depolymerize into cyclooctene (Fig. 3d) despite a reduction in molecular weight (Supplementary Fig. 17). Moreover, the ROMP polymers of both *cis*- and *trans*-cyclopropane-fused cyclooctenes at the 5 and 6 positions (*cis*-*g*DCC-CO and *trans*-*g*DCC-CO, respectively) did not depolymerize into the corresponding monomers (Fig. 3e,f), which is consistent with the high RSEs of these monomers (Fig. 1b). In addition, a 1,9-decadiene with *trans*-cyclobutane installed at its 5 and 6 positions underwent RCM at quantitative conversion to form *t*CBCO when it was refluxed in the presence of **G2** (Supplementary Fig. 18). By contrast, when the *cis*-cyclobutane diene was subjected to the same conditions, no *cis*-cyclobutane-fused cyclooctene was observed in the mass spectrum, which instead showed a mixture of acyclic and cyclic oligomers (Supplementary Figs. 19–21). The depolymerization and RCM studies confirm the computational results that *trans*-cyclobutane appreciably reduces the RSE of cyclooctene and highlight the impact of the size and stereochemistry of the fused ring on the RSE of a cyclic molecule.

The depolymerization conditions, including temperature and concentration, were screened in order to understand the thermodynamics and to identify the optimal conditions for depolymerization. Conversions of 94–98% were obtained when the depolymerization of **P2a** was conducted at concentrations of [olefin] ≤ 200 mM at 50 °C (Supplementary Table 1). In particular, the concentration of 200 mM corresponds to a weight concentration of 5% (w/w), meaning that 5 g of polymers can be depolymerized using 100 ml of

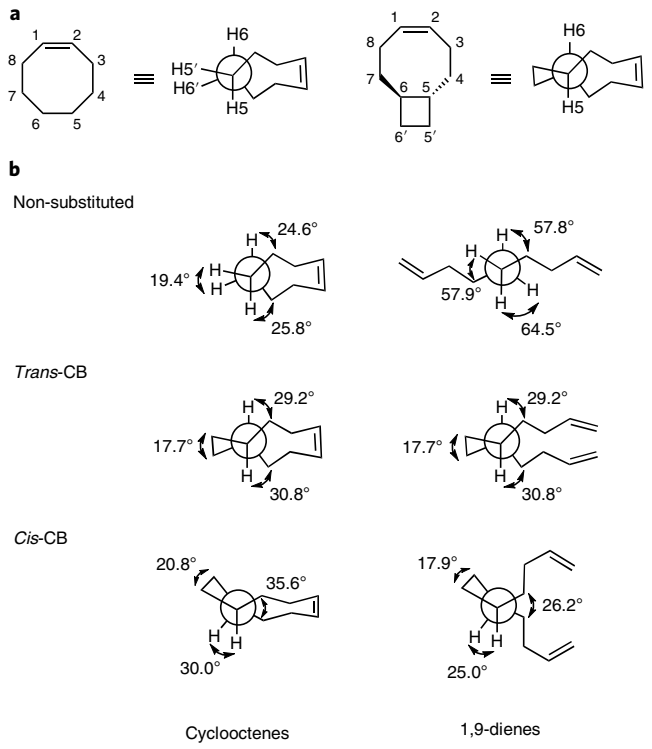

Fig. 4 | Newman projections along the C5–C6 bond for 1,9-dienes and cyclooctenes. a, The structures and corresponding Newman projections of cyclooctene and *trans*-cyclobutane-substituted cyclooctene showing the numbering scheme used here. **b**, The projections for non-substituted, *trans*-cyclobutane (*trans*-CB)-substituted and *cis*-cyclobutane (*cis*-CB)-substituted 1,9-dienes and cyclooctenes. The dihedral angles H5–C5–C6–C7 and H6–C6–C5–C4, as well as H5′–C5–C6–H6′ (for the case with no substitution) and C5′–C5–C6–C6′ (for the cases involving CB substitution), are shown along with the projections.

solvent, which adds to the practicality of the chemical recycling. The conversion of depolymerization became more sensitive to concentration at [olefin] ≥ 200 mM. For example, the conversions dropped to 84% and 66%, respectively, when the concentrations increased to 400 mM and 600 mM. Temperature plays a lesser role in determining the final conversion of the depolymerization. For example, the depolymerization conversions at 50 °C for [olefin] = 100 mM and 400 mM were 97% and 84%, respectively, and the corresponding values at 19 °C were 94% and 85% (Supplementary Table 1). The insensitivity to temperature of the equilibrium depolymerization conversion is consistent with the low entropy change of the reaction, as discussed above.

To understand the depolymerization process, depolymerization of **P2a** was conducted at three different temperatures (50 °C, 45 °C and 19 °C) and was monitored with ^{1}H NMR and GPC. The GPC traces (Supplementary Figs. 22–24) suggest that both the monomer (retention time, 19.7–21.5 min) and oligomers (retention time, 17.7–19.7 min) formed during depolymerization. The formation of oligomers during depolymerization is also supported by MS characterization (Supplementary Figs. 10, 11 and 25). The fraction of the oligomers was obtained from the integration of the GPC refactive index (RI) traces (details in Supplementary Information). When the depolymerization was conducted at 50 °C, no residual polymer peak was observed after 3 min. This rapid depolymerization makes it inconvenient to obtain sufficient data points for kinetic studies (Supplementary Fig. 22). The time after which no residual polymer was observed was 10 min at 45 °C (Supplementary Fig. 23) and 120 min at 19 °C (Supplementary Fig. 24), which allowed sufficient data points to be obtained for kinetic analysis. The fractions of monomer, oligomers and residual polymer were plotted against depolymerization time for depolymerization at 45 °C (Supplementary Fig. 23) and 19 °C (Supplementary Fig. 24). As shown in the plots, the polymer fraction continuously decreased while the monomer fraction continuously increased throughout depolymerization. However, the fraction of oligomers first increased and reached a maximum in the range of ~30–40% before starting to decrease (Supplementary Fig. 23 and 24). Most of the oligomers eventually turned into the monomer. For example, no residual polymer was observed for the depolymerization of **P2a** at 45 °C at 10 min; at that time, the fractions of monomer and oligomer were 80% and 20%, respectively. The oligomers continued to convert into monomer until an equilibrium was reached at around 20 min. The equilibrium fractions for monomer and oligomers were 93% and 7%, respectively. In addition, when the depolymerization was conducted at 19 °C, the fractions of the oligomers were higher than those of the monomer at the early stage of depolymerization (0–30 min). These results suggest that while the monomer is the thermodynamic products, the formation of the oligomers is kinetically more favourable. The formation of cyclic oligomers was not observed for the depolymerization of polypentenamers[35]. This difference can be attributed to the difference between the RSEs of the monomer and dimer: the difference in RSE between the eight-membered and sixteen-membered rings might be less drastic than that between the five-membered and ten-membered rings.

Studies by Badamshina et al. showed that the depolymerization of polypentenamer proceeds through a random chain cleavage pathway[36]. Recently, Kennemur and coworkers studied the depolymerization mechanism of a bottlebrush polypentenamer and found that the chain cleavage occurs in an end-to-end fashion[35]. In this case, due to the steric hinderance of the side chain in the bottlebrush, the ruthenium catalyst preferentially coordinates to the terminal olefin over the internal olefin. Since there is no long side chain in the linear *t*CBCO polymers, it is expected that the depolymerization will proceed in a random fashion, similar to that for a linear polypentenamer. At the early stage of depolymerization, the polymer peak shifted to a longer retention time; meanwhile, a shoulder peak that connects the polymer peak and the oligomer peaks appeared (Supplementary Figs. 22–24). The shoulder peak eventually disappeared along with the polymer peak. The appearance of a shoulder peak supports random chain cleavage, since a shoulder peak is not expected for the end-to-end depolymerization[35]. In addition, end-to-end depolymerization would result in a linear reduction of molecular weight over the fraction of depolymerization; however, the plot of molecular weight against depolymerization conversion did not show a linear relationship (Supplementary Figs. 23 and 24), further suggesting that random chain cleavage occurred during the depolymerization.

Structure and RSE relationships. The finding that the ring strain of cyclooctene is reduced by a highly strained cyclobutane is somewhat counterintuitive. Transannular strain and torsional strain are important sources of ring strain in medium-sized (seven- to twelve-membered) rings[37,38]. To assess the impact of the cyclobutane-fused ring on the transannular interaction, we looked at all of the non-bonded H–H distances on the unsubstituted cyclooctene and *t*CBCO. The list of the H–H distances in Supplementary Fig. 26 shows that only one notable transannular interaction is present in the unsubstituted cyclooctene: it occurs between H3a and H8a at a distance of 2.15 Å. Incorporation of a *trans*-cyclobutane-fused ring only slightly increases the H3a–H8a distance (2.18 Å), indicating that the transannular strain is not noticeably impacted by the *trans*-cyclobutane-fused ring. Since the ring strain of a cyclic molecule is the relative energy between the cyclic molecule and an acyclic reference molecule, to understand the impact of the fused rings

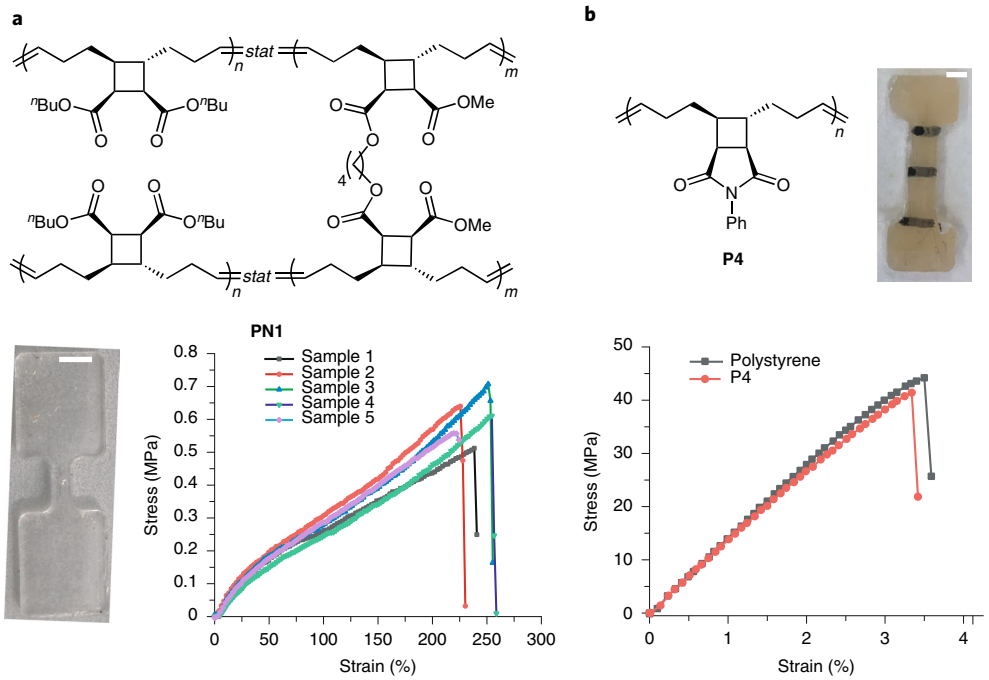

Fig. 5 | Mechanical properties of *t*CBCO polymers. a, Chemical structure of the *t*CBCO-based elastomer **PN1**, a photo of the dog-bone specimen of **PN1** (scale bar, 2 mm) and stress–strain curve obtained from the tensile test (5 mm min^{-1}, room temperature) for **PN1**. **b**, Chemical structure of the glassy polymer **P4**, a photo of dog-bone specimen (scale bar, 2 mm) of **P4** and stress–strain curves for **P4** (in red) and polystyrene (in grey) obtained from tensile test (5 mm min^{-1}, room temperature).

on the ring strain, we examined the structural difference between the cyclooctenes and the acyclic 1,9-decadienes (the structures of which were obtained for use in the ring strain calculations) via the Newman projection along the C5–C6 bond (Fig. 4). The dihedral angles H5–C5–C6–C7, H6–C6–C5–C4 and H5′–C5–C6–H6′ in cyclooctene are 25.8°, 24.6° and 19.4°, respectively, generating substantial torsional strain. The torsional strain becomes negligible in the acyclic 1,9-diene, as the dihedral angles are all close to 60°. We then looked at the *trans*-cyclobutane-fused cyclooctene, in which the H5′ and H6′ (of an unsubstituted cyclooctene) are replaced with C5′ and C6′. As shown in Fig. 4, the dihedral angles H5–C5–C6–C7, H6–C6–C5–C4 and C5′–C5–C6–C6′ in *t*CBCO are 30.8°, 29.2° and 17.7°, respectively. Notably, these dihedral angles remain identical in the corresponding acyclic diene. As a result, the relative energy between *t*CBCO and the corresponding acyclic diene is reduced. As for the *cis*-cyclobutane-fused system, while torsional strain is also present in the acyclic diene, the dihedral angles are markedly different from those in the cyclic form, indicating that the structure of cyclobutane is distorted from the acyclic to the cyclic olefin. The reduction of ring strain by maintaining the eclipsing effect in the acyclic form is therefore offset by the distortion energy in the case of *cis*-cyclobutane-fused cyclooctene. The compensation between these two effects can be generalized to other cycloalkane-fused cyclooctenes: while the cycloalkanes (from three- to six-membered rings) reduce the ring strain by locking the conformation of the acyclic form so that the eclipsing effect is present (Supplementary Figs. 27 and 28), the fusion of the two rings (the cycloalkane and cyclooctene) can distort the cycloalkane, which increases the ring strain. As shown in Supplementary Fig. 29, the RSEs of the cycloalkane-fused cyclooctenes correlate well with the distortion of the dihedral angles C4–C5–C5′–C6 and C7–C6–C6′–C5 from the acyclic diene to cycloalkane-fused cyclooctene. The *trans*-cyclobutane therefore represents an ideal scenario where the torsional strain is maintained in both the cyclic and acyclic forms at a low energy cost.

Thermal and mechanical properties. The mild depolymerization conditions along with the excellent thermal stability (T_d > 370 °C) of the *t*CBCO polymers make them appealing for use as sustainable materials. Since a wide range of T_g values (from −30 °C to 100 °C) can be accessed through functionalization of the *t*CBCO polymers (Fig. 2b), both elastomers and plastics can be prepared. Using the monomer **M2b** (T_g of **P2b** is −31 °C) and a *t*CBCO crosslinker **XL1** (for the structure and characterization, Supplementary Information), we prepared an elastomer **PN1** and conducted a tensile test (Fig. 5a). The stress–strain curve showed a Young's modulus of 0.61 ± 0.10 MPa, a maximum strain of 238 ± 15% and a tensile strength of 0.61 ± 0.10 MPa. Previous work by Moore and coworkers has shown that metathesis-based depolymerization can occur in bulk materials, suggesting that the crosslinked material here should still be depolymerizable[39]. A depolymerization conversion of 94% was observed when **PN1** was immersed in a solution of **G2** in $CDCl_3$ and was heated to 50 °C for 2 h (Supplementary Fig. 30).

The imide-functionalized *t*CBCO polymer **P4** has a T_g of 100 °C (Fig. 2b), which is comparable to that of polystyrene (one of the most widely used plastics). The large thermal processing window (which is above the T_g but below the T_d) of **P4** allowed the melt-pressing of films of the material. From the melt-pressed film of **P4**, we prepared a dog-bone specimen and conducted tensile testing to obtain the stress–strain curve (Fig. 5b). A polystyrene sample was processed in the same manner and was subjected to tensile testing for comparison. As shown in Fig. 5b, **P4** showed a Young's modulus of 1.40 ± 0.06 GPa, which is comparable to that of polystyrene (1.56 ± 0.12 GPa). The strain at break (3.4 ± 0.3%) and the tensile strength (39 ± 5 MPa) of **P4** were also comparable to those of polystyrene (strain at break of 3.7 ± 0.4% and a tensile strength of 46 ± 1 MPa).

Conclusions

In principle, the *t*CBCO monomers can be obtained by the photochemical [2 + 2] cycloaddition of 1,5-cyclooctadiene with a wide

variety of olefins, therefore providing numerous possibilities of functionalities and material properties. For example, this process would enable the preparation of chemically recyclable polymers using biobased olefins[40], therefore reducing the reliance on fossil feedstocks. Another example is the use of fluorinated olefins for preparing chemically recyclable fluorinated polymers, which are highly desirable but particularly rare. Moreover, the *cis*-alkene in the cyclooctene monomer can be isomerized into *trans*-alkene, which substantially increases the ring strain of the monomer, allowing for living polymerization. This feature (temporarily increasing the monomer ring strain to assist polymerization) makes the *t*CBCO system unique compared to other depolymerization systems[6]. The living ROMP of norbornene-derived monomers has enabled the synthesis of diverse polymer architectures and has fundamentally impacted many fields[41]; however, the resulting polynorbornenes are not depolymerizable. The *t*CBCO system will allow for living ROMP that produces depolymerizable polymers. Furthermore, the concept of controlling ring strain using an additional ring—as well as the insights gained in this study on how the size and stereochemistry of the fused ring impact the ring strain—can be useful for many other fields where ring strain plays an important role, including mechanochemistry[42], molecular machines[43], catalysis[44] and click chemistry[45]. For example, in the strain-promoted azide–alkyne cycloaddition demonstrated by Bertozzi and coworkers, the reactivity is substantially increased by the ring strain in cyclooctyne[45]. The fused-ring strategy used here could be applied to further control the ring strain of cyclooctyne and the strain-promoted azide–alkyne cycloaddition reactivity.

Online content

Any methods, additional references, Nature Research reporting summaries, source data, extended data, supplementary information, acknowledgements, peer review information; details of author contributions and competing interests; and statements of data and code availability are available at https://doi.org/10.1038/s41557-021-00748-5.

Received: 28 September 2020; Accepted: 10 June 2021;
Published online: 22 July 2021

References

1. Rochman, C. M. et al. Classify plastic waste as hazardous. *Nature* **494**, 169–171 (2013).
2. *The New Plastics Economy: Rethinking the Future of Plastics and Catalysing Action* (Ellen MacArthur Foundation, 2017).
3. Haider, T. P., Völker, C., Kramm, J., Landfester, K. & Wurm, F. R. Plastics of the future? The impact of biodegradable polymers on the environment and on society. *Angew. Chem. Int. Ed.* **58**, 50–62 (2019).
4. Ignatyev, I. A., Thielemans, W. & Vander Beke, B. Recycling of polymers: a review. *ChemSusChem* **7**, 1579–1593 (2014).
5. Tang, X. & Chen, E. Y. X. Toward infinitely recyclable plastics derived from renewable cyclic esters. *Chem* **5**, 284–312 (2019).
6. Coates, G. W. & Getzler, Y. D. Y. L. Chemical recycling to monomer for an ideal, circular polymer economy. *Nat. Rev. Mater.* **5**, 501–516 (2020).
7. Snow, R. D. & Frey, F. E. The reaction of sulfur dioxide with olefins: the ceiling temperature phenomenon. *J. Am. Chem. Soc.* **65**, 2417–2418 (1943).
8. Dainton, F. S. & Ivin, K. J. Reversibility of the propagation reaction in polymerization processes and its manifestation in the phenomenon of a 'ceiling temperature'. *Nature* **162**, 705–707 (1948).
9. McCormick, H. W. Ceiling temperature of α-methylstyrene. *J. Polym. Sci.* **25**, 488–490 (1957).
10. North, A. M. & Richardson, D. Entropy of stereoregularity in aldehyde polymerization. *Polymer* **6**, 333–338 (1965).
11. Park, C. W. et al. Thermally triggered degradation of transient electronic devices. *Adv. Mater.* **27**, 3783–3788 (2015).
12. Feinberg, A. M. et al. Cyclic poly(phthalaldehyde): thermoforming a bulk transient material. *ACS Macro Lett.* **7**, 47–52 (2018).
13. Tran, H. et al. Stretchable and fully degradable semiconductors for transient electronics. *ACS Cent. Sci.* **5**, 1884–1891 (2019).
14. Zhu, J.-B., Watson, E. M., Tang, J. & Chen, E. Y. X. A synthetic polymer system with repeatable chemical recyclability. *Science* **360**, 398–403 (2018).
15. Grubbs, R. H. Olefin metathesis. *Tetrahedron* **60**, 7117–7140 (2004).
16. Grubbs, R. H. & Khosravi, E. *Handbook of Metathesis: Polymer Synthesis* 2nd edn, Vol. 3 (Wiley, 2015).
17. Monfette, S. & Fogg, D. E. Equilibrium ring-closing metathesis. *Chem. Rev.* **109**, 3783–3816 (2009).
18. Neary, W. J. & Kennemur, J. G. Polypentenamer renaissance: challenges and opportunities. *ACS Macro Lett.* **8**, 46–56 (2019).
19. Myers, S. B. & Register, R. A. Synthesis of narrow-distribution polycyclopentene using a ruthenium ring-opening metathesis initiator. *Polymer* **49**, 877–882 (2008).
20. Neary, W. J. & Kennemur, J. G. Variable temperature ROMP: leveraging low ring strain thermodynamics to achieve well-defined polypentenamers. *Macromolecules* **50**, 4935–4941 (2017).
21. Schleyer, P. v. R., Williams, J. E. & Blanchard, K. R. Evaluation of strain in hydrocarbons. The strain in adamantane and its origin. *J. Am. Chem. Soc.* **92**, 2377–2386 (1970).
22. Hejl, A., Scherman, O. A. & Grubbs, R. H. Ring-opening metathesis polymerization of functionalized low-strain monomers with ruthenium-based catalysts. *Macromolecules* **38**, 7214–7218 (2005).
23. Martinez, H., Ren, N., Matta, M. E. & Hillmyer, M. A. Ring-opening metathesis polymerization of 8-membered cyclic olefins. *Polym. Chem.* **5**, 3507–3532 (2014).
24. Walker, R., Conrad, R. M. & Grubbs, R. H. The living ROMP of trans-cyclooctene. *Macromolecules* **42**, 599–605 (2009).
25. You, W., Padgett, E., MacMillan, S. N., Muller, D. A. & Coates, G. W. Highly conductive and chemically stable alkaline anion exchange membranes via ROMP of trans-cyclooctene derivatives. *Proc. Natl Acad. Sci. USA* **116**, 9729–9734 (2019).
26. You, W., Hugar, K. M. & Coates, G. W. Synthesis of alkaline anion exchange membranes with chemically stable imidazolium cations: unexpected cross-linked macrocycles from ring-fused ROMP monomers. *Macromolecules* **51**, 3212–3218 (2018).
27. Scherman, O. A., Walker, R. & Grubbs, R. H. Synthesis and characterization of stereoregular ethylene-vinyl alcohol copolymers made by ring-opening metathesis polymerization. *Macromolecules* **38**, 9009–9014 (2005).
28. Hsu, T.-G. et al. A polymer with "locked" degradability: superior backbone stability and accessible degradability enabled by mechanophore installation. *J. Am. Chem. Soc.* **142**, 2100–2104 (2020).
29. Asaoka, S., Horiguchi, H., Wada, T. & Inoue, Y. Enantiodifferentiating photocyclodimerization of cyclohexene sensitized by chiral benzenecarboxylates. *J. Chem. Soc. Perkin Trans.* **2**, 737–747 (2000).
30. Maeda, H. et al. Synthesis and photochemical properties of stilbenophanes tethered by silyl chains. Control of (2π + 2π) photocycloaddition, cis−trans photoisomerization, and photocyclization. *J. Org. Chem.* **70**, 9693–9701 (2005).
31. Xu, Y., Smith, M. D., Krause, J. A. & Shimizu, L. S. Control of the intramolecular [2+2] photocycloaddition in a bis-stilbene macrocycle. *J. Org. Chem.* **74**, 4874–4877 (2009).
32. Poplata, S., Tröster, A., Zou, Y.-Q. & Bach, T. Recent advances in the synthesis of cyclobutanes by olefin [2+2] photocycloaddition reactions. *Chem. Rev.* **116**, 9748–9815 (2016).
33. Feist, J. D. & Xia, Y. Enol ethers are effective monomers for ring-opening metathesis polymerization: synthesis of degradable and depolymerizable poly(2,3-dihydrofuran). *J. Am. Chem. Soc.* **142**, 1186–1189 (2020).
34. Royzen, M., Yap, G. P. A. & Fox, J. M. A photochemical synthesis of functionalized trans-cyclooctenes driven by metal complexation. *J. Am. Chem. Soc.* **130**, 3760–3761 (2008).
35. Neary, W. J., Isais, T. A. & Kennemur, J. G. Depolymerization of bottlebrush polypentenamers and their macromolecular metamorphosis. *J. Am. Chem. Soc.* **141**, 14220–14229 (2019).
36. Badamshina, E. R. et al. Investigation of the mechanism of polypentenamer degradation in the presence of metathesis catalysts. *Polym. Sci. USSR* **24**, 164–170 (1982).
37. Prelog, V. Conformation and reactivity of medium-sized ring compounds. *Pure Appl. Chem.* **6**, 545–560 (1963).
38. Burevschi, E., Peña, I. & Sanz, M. E. Medium-sized rings: conformational preferences in cyclooctanone driven by transannular repulsive interactions. *Phys. Chem. Chem. Phys.* **21**, 4331–4338 (2019).
39. Liu, H. et al. Dynamic remodeling of covalent networks via ring-opening metathesis polymerization. *ACS Macro Lett.* **7**, 933–937 (2018).
40. Stalpaert, M. et al. Olefins from biobased sugar alcohols via selective, ru-mediated reaction in catalytic phosphonium ionic liquids. *ACS Catal.* **10**, 9401–9409 (2020).
41. Sutthasupa, S., Shiotsuki, M. & Sanda, F. Recent advances in ring-opening metathesis polymerization, and application to synthesis of functional materials. *Polym. J.* **42**, 905–915 (2010).

42. Caruso, M. M. et al. Mechanically-induced chemical changes in polymeric materials. *Chem. Rev.* **109**, 5755–5798 (2009).
43. Feringa, B. L. The art of building small: from molecular switches to motors (Nobel Lecture). *Angew. Chem. Int. Ed.* **56**, 11060–11078 (2017).
44. Walczak, M. A. A., Krainz, T. & Wipf, P. Ring-strain-enabled reaction discovery: new heterocycles from bicyclo[1.1.0]butanes. *Acc. Chem. Res.* **48**, 1149–1158 (2015).
45. Agard, N. J., Prescher, J. A. & Bertozzi, C. R. A strain-promoted [3 + 2] azide–alkyne cycloaddition for covalent modification of biomolecules in living systems. *J. Am. Chem. Soc.* **126**, 15046–15047 (2004).

Methods

Calculations of RSEs. The RSEs of the cyclic olefins were calculated by following a method demonstrated by Grubbs and coworkers[22]. This method involves the calculation of the enthalpy change for the ring-closing metathesis (Fig. 1c). Since the numbers and types of bonds of the reactant are identical to those of the products (that is, an isodesmic reaction), the enthalpy change of the reaction should come solely from the change in ring strain (equation (1))—which is essentially the ring strain of the cyclic olefin, as there is no ring strain in the acyclic diene reactant or the ethylene products.

$$\mathrm{RSE} = \Delta H = H_{\mathrm{ethene}} + H_{\mathrm{cyclic\ olefin}} - H_{\mathrm{diene}} \quad (1)$$

H_{ethene}, $H_{\mathrm{cyclic\ olefin}}$ and H_{diene} are the calculated ethalpies at 298.15 K and 1.0 atm for ethene, the cyclic olefin and the diene, respectively. All calculations were performed using Gaussian 16 at the B3LYP/6-31G(d,p) level of theory. The structures were first optimized with the Universal Force Field as implemented in the auto-optimization tool in Avogadro, followed by a conformer search with Avogadro, and the optimized conformation was subjected to geometry optimization and vibrational frequency calculations using Gaussian 16.

Thermodynamics studies of polymerization. Thermodynamics studies were performed for the diester monomer **M2a** and imide monomer **M4**. The polymerization for **M2a** was conducted at five different temperatures, and the polymerization for **M4** was conducted at four different temperatures. The equilibrium monomer concentration $[M]_e$ for each temperature was measured via ^{1}H NMR. The thermodynamic parameters were obtained by plotting $\ln[M]_e$ against temperature $1/T$ (van't Hoff plot) according to equation (2):

$$\ln[M]_e = \frac{\Delta H}{RT} - \frac{\Delta S}{R} \quad (2)$$

In equation (2), $[M]_e$ is the equilibrium monomer concentration in moles per litre, T is the reaction temperature in Kelvin (K), ΔH is the enthalpy of reaction in kilocalories per mole, ΔS is the entropy of reaction in calories per mole per Kelvin and R is the gas constant, 8.314 J mol^{-1} K^{-1}. The values for ΔH and ΔS can be obtained from the slope and the intercept of the van't Hoff plot, respectively. The following procedure is a representative example of the polymerization performed here.

M2a (252.3 mg, 1.0 mmol, 1 equiv.) was dissolved in 0.5 ml xylene in a 1 ml volumetric flask. Additional xylene was added to reach the 1 ml mark to form the 1 M monomer solution, which was transferred to a 1 dram vial. To the monomer solution was added **G2** (8.5 mg, 0.01 mmol, 0.01 equiv.); 200 µl of the solution was added to each of another four vials, and the five vials were placed in five oil baths that were preheated to the desired temperatures. Since time studies of the polymerization show that the polymerization would have reached equilibrium before 7 h (Supplementary Figs. 32–34), the reactions were quenched at 7 h with ethyl vinyl ether (100 µl) and the conversion was measured with ^{1}H NMR. The olefinic peaks in the ^{1}H NMR for the monomer and polymer were integrated to determine the residual monomer content at equilibrium (Supplementary Fig. 83).

Supplementary Figs. 1 and 2 contain the equilibrium monomer concentration for polymerization of **M2a** and **M4** at various temperatures (averaged over three runs), respectively. From the van 't Hoff plot for **M2a** (Supplementary Fig. 1), a slope of −861.46 and an intercept of 1.824 were obtained. The enthalpy change and entropy change of the reaction were calculated as follows:

$$\frac{\Delta H}{R} = -861.46$$

$$-\frac{\Delta S}{R} = 1.824$$

The calculation resulted in $\Delta H = -1.7$ kcal mol^{-1} and $\Delta S = -3.6$ cal mol^{-1} K^{-1} for **M2a**. Similarly, for **M4**, $\Delta H = -2.8$ kcal mol^{-1} and $\Delta S = -4.9$ cal mol^{-1} K^{-1} were obtained (Supplementary Fig. 2).

Depolymerization studies. A representative depolymerization procedure is given as follows: in a vial equipped with a stir bar, **P2a** (146.5 mg, 0.58 mmol, 1 equiv.) was dissolved in $CHCl_3$ (5 ml). To the polymer solution was added **G2** (4.93 mg, 0.0058 mmol, 0.01 equiv.) from a stock solution. The volume of the added **G2** solution was precalculated to obtain a concentration of 25 mM ([olefin] = 25 mM). The vial was placed in an oil bath preheated to 50 °C and stirred for 2 h. Then 0.5 ml ethyl vinyl ether was added to quench the reaction, and the mixture was stirred for 15 min. The vial was allowed to cool to room temperature, and 930 mg of Quadrapure TU macroporous particles and 1 ml $CHCl_3$ were added. The mixture was stirred overnight, after which it was filtered through a Celite plug. The filtrate was concentrated on a rotary evaporator and characterized using ^{1}H NMR and GPC. The initial molecular weight and concentration as well as the extent of conversion to monomer for each polymer are shown in Supplementary Table 1.

Mechanical testing. The tensile testing experiments were performed on five parallel specimens for both the elastomer (**PN1**) and the two plastics (polystyrene and **P4**). The values of mechanical properties are reported as average plus or minus standard deviation.

Tensile testing of the elastomer sample **PN1** was performed on a custom-built tensile tester controlled by an Arduino UNO board. A crosshead speed of 5 mm min^{-1} was used. For the tensile testing of **P4**, a dichloromethane solution of the polymer was allowed to dry under ambient conditions followed by drying in a vacuum oven at 110–120 °C for 2 days, until no further mass change occured. Dog-bone-shaped samples of gauge length 10 × 3 × 1.5 mm^3 were prepared by compression moulding using a Carver Lab Press at zero pressure for 3 min at 130–150 °C, followed by 9,000 kg pressure for 5 min at the same temperature. Samples were then quenched in water and allowed to equilibrate for an hour at room temperature prior to examination of the mechanical properties. Dog-bone specimens made from Styron 663 polystyrene (acquired from Dow Chemical) were prepared by following a similar procedure for comparison. Mechanical properties were determined at a constant speed of 5 mm min^{-1} using an Instron 5969 tensile tester, which gave an initial crosshead speed V/L_0 of 0.5 min^{-1}, where V is the pulling speed and L_0 is the initial length.

Data availability

Crystallographic data for the structures in this Article have been deposited at the Cambridge Crystallographic Data Centre (CCDC) under deposition nos 2032007 (**2**), 2032008 (**6**) and 2032009 (**10**). Copies of data can be obtained free of charge from www.ccdc.cam.ac.uk/structures/. All other data supporting the findings of this study are available within the Article and its Supplementary Information. Source data are provided with this paper.

Acknowledgements

This work is supported by the University of Akron. The computational resources were provided by Extreme Science and Engineering Discovery Environment (TG-CHE190099). The single-crystal structures were characterized with an X-ray diffractometer supported by the National Science Foundation (CHE-0840446 to C.J.Z.). We thank S. Wang for helpful discussion and K. Williams-Pavlantos and C. Wesdemiotis for conducting the MS analysis.

Author contributions

J.W. conceived the project and directed the research. D.S. and J.W. performed the density functional theory calculations and analysed the computational data. D.S., J.Z., H.C., W.X., H.-W.S. and T.-G.H. conducted the monomer and polymer syntheses. B.R.S. and C.J.Z. collected and analysed the single-crystal data. D.S. and W.X. conducted the thermodynamic studies and depolymerization. J.Z. conducted the ring-closing metathesis experiments. D.S. and J.Z. conducted the thermal characterization of the polymers. D.S. and T.S. conducted mechanical testing. D.S. and J.W. prepared the manuscript.

Competing interests

The authors declare no competing interests.

Additional information

Supplementary information The online version contains supplementary material available at https://doi.org/10.1038/s41557-021-00748-5.

Correspondence and requests for materials should be addressed to J.W.

Peer review information *Nature Chemistry* thanks Frank Leibfarth and the other, anonymous, reviewer(s) for their contribution to the peer review of this work.

Reprints and permissions information is available at www.nature.com/reprints.